THE UNIVERSITY of EDINBURGH

Edinburgh Research Explorer

Adrenal gland tumorigenesis after gonadectomy in mice is a complex genetic trait driven by epistatic loci

OPEN ACCESS

Adrenal Gland Tumorigenesis after Gonadectomy in Mice Is a Complex Genetic Trait Driven by Epistatic Loci

Sophie Bernichtein, **Enrico Petretto**, **Stacey Jamieson**, **Anuj Goel**, **Timothy J. Aitman**, **Jonathan M. Mangion**, and **Ilpo T. Huhtaniemi**

Department of Reproductive Biology (S.B., S.J., I.T.H.); Physiological Genomics and Medicine Group (E.P., A.G., T.J.A., J.M.M.), Medical Research Council, Clinical Sciences Center; Division of Epidemiology (E.P.), Public Health and Primary Care; and Section of Molecular Genetics and Rheumatology (T.J.A.), Faculty of Medicine, Imperial College London, London W12 0NN, United Kingdom

Abstract

Postgonadectomy adrenocortical tumorigenesis is a strain-specific phenomenon in inbred mice, assumed to be caused by elevated LH secretion and subsequent ectopic LH receptor (LHR) overexpression in adrenal gland. However, the molecular mechanisms of this cascade of events remain unknown. In this study, we took advantage of the mouse strain dependency of the phenotype to unravel its genetic basis. Our results present the first genome-wide screening related to this pathology in two independent F2 and backcross populations generated between the neoplastic DBA/2J and the nonsusceptible C57BL/6J strains. Surprisingly, the postgonadectomy elevation of serum LH was followed by similar up-regulation of adrenal LHR expression in both parental strains and their crosses, irrespective of their tumor status, indicating that it is not the immediate cause of the tumorigenesis. Linkage analysis revealed one major significant locus for the tumorigenesis on chromosome 8, modulated by epistasis with another quantitative trait locus on chromosome 18. Weight gain, a secondary phenotype after gonadectomy, showed a significant but separate quantitative trait locus on chromosome 7. Altogether, postgonadectomy adrenocortical tumorigenesis in DBA/2J mice is a dominant trait that is not a direct consequence of adrenal LHR expression but is driven by a complex genetic architecture. Analysis of candidate genes in the tumorigenesis linkage region showed that *Sfrp1* (secreted frizzled-related protein 1), a tumor suppressor gene, is differentially expressed in the neoplastic areas. These findings may have relevance to the human pathogenesis of macronodular adrenal hyperplasia and adrenocortical tumors in postmenopausal women and why some of them develop obesity.

The molecular pathogenesis of adrenal tumors is poorly understood (1), as exemplified by human adrenal incidentalomas, which are a common opportune finding (2). Interestingly, adrenal gland neoplasms often develop after gonadal failure and chronic gonadotropin elevation, as in postmenopausal women (3,4) or in men with acquired primary hypogonadism (5). The connection between the gonadal and adrenal pathologies remains elusive, but conspicuously, a subset of the adrenal tumors are gonadotropin responsive (6,7). Likewise, in ACTH-independent Cushing's syndromes, the adrenals of some patients have been reported to be gonadotropin responsive (8). Moreover, rare cases of pregnancy-associated Cushing's syndrome with adrenal hyperfunction related to elevated human chorionic gonadotropin levels have been described (9). Another clinical syndrome of relevance is the macronodular adrenal

Address all correspondence and requests for reprints to: Ilpo Huhtaniemi, Institute of Reproductive and Developmental Biology, Faculty of Medicine, Imperial College London, Hammersmith Campus, Du Cane Road, London W12 0NN, United Kingdom. E-mail: ilpo.huhtaniemi@imperial.ac.uk..

hyperplasia, where ectopic G protein-coupled receptor expression, *e.g.* of the LH receptor (LHR), is a pathognomonic finding (8).

The connection between high gonadotropin levels and adrenocortical pathologies is clearer in some mammalian models. For example, neutered ferrets develop with high frequency the syndrome of gonadotropin-induced adrenocortical neoplasia with associated Cushingoid obesity (10). Studies on genetically modified mice have revealed that the etiology of these pathologies is due to a combination of genetic and hormonal factors (11-13). Excessive LH levels, induced by ovariectomy (Ovx) or transgenic LH overexpression, lead to ectopic LHR overexpression in the adrenal gland, followed by adrenocortical hyperplasia or tumorigenesis (14,15). However, the exact molecular mechanisms leading to this apparent gonadotropin-dependent adrenocortical neoplasia remain unknown.

In addition, the postgonadectomy tumorigenesis in mice occurs only in specific inbred strains, indicating a clear genetic component in this response. It is well recognized that only certain mouse strains (*e.g.* DBA/2J and CE/J) develop adrenocortical neoplasms in response to prepubertal Ovx with high penetrance, whereas other nonsusceptible strains (*e.g.* C57BL/6J and FVB/N) never develop them (16,17). Organ transplantation experiments have established that the adrenal glands of susceptible strains exhibit an inherent predisposition for tumor formation in response to the hormonal changes after Ovx, but the genetic basis of this susceptibility is unknown.

After Ovx, DBA/2J females exhibit high serum LH levels, with subsequent development of adrenocortical tumors that overexpress LHR and the transcription factor GATA-4 (14). The adrenocortical neoplasms originate by proliferation of small spindle-shaped cells (termed A cells) in the subcapsular region (16). More advanced neoplasia is defined by nests of round steroidogenic lipid-laden cells, termed B cells, among the A cells (18). Interestingly, along with tumorigenesis, DBA2/J mice also develop obesity, reminiscent of Cushing's syndrome of postmenopausal women.

We hypothesized that the high penetrance and strict strain dependence of the gonadectomy-induced adrenal tumors provide the basis for a genetic approach to identify the genomic regions related to, and genes responsible for, the pathogenesis.

In the present study, we describe the first genetic approach to explore the molecular pathogenesis of postgonadectomy (or gonadotropin-induced) adrenal gland tumorigenesis and obesity in two selected strains of mice by performing a genome-wide screen in segregating populations derived from the nonsusceptible C57BL/6J and the susceptible DBA/2J strains. We report that epistasis between quantitative trait loci (QTL) is an important contributor to the genetics of mouse adrenocortical tumorigenesis and that this pathology could be regarded as a complex genetic trait. *Sfrp1* (secreted frizzled-related protein 1), a tumor suppressor gene, is a positional candidate gene that could be proposed as one of the biological candidate genes in the induction of the adrenal tumors.

Materials and Methods

Experimental animals and treatments

All animal work was carried out in accordance to the United Kingdom Home Office Project License and the personal licenses held by the authors. Mice of inbred strains DBA/2J and C57BL/6J were purchased from Charles River Laboratories UK (Kent, UK), and all mice were kept in specific pathogen-free conditions in controlled conditions of light and temperature and fed with standard laboratory animal food and water *ad libitum*.

Fifty F1 progeny were generated by crossing DBA/2J with C57BL/6J, and intercrosses between F1 animals produced 208 F2 females for the linkage study. Twenty-five F1 females were also backcrossed with C57BL/6J males to generate 125 backcross (BC) females used for the linkage.

Prepubertal Ovx was performed at 21–24 d of age. Isoflurane inhalation anesthesia was used during surgical procedures, and buprenorphine was used as postoperative analgesia. All mice produced (including F2 and BC mice), had postgonadectomy WG monitored every month up to the time of termination, and the final WG at 6 months upon Ovx was taken for the linkage study. The same F2 and BC mice were assessed for their adrenal tumor status (TS) as described in *Adrenocortical tumor assessment* below. At specified times after surgery (up to 6 months for the linkage studies), mice were killed by CO_2 inhalation. Blood samples were obtained at the time of death. At autopsy, several tissues including liver and adrenals were dissected out and snap-frozen in liquid nitrogen or fixed in neutral formalin solution overnight before embedding in paraffin and sectioned (6 μm) for staining with hematoxylin-eosin or for immunohistochemistry experiments. Some harvested adrenals were also used to isolate total RNA using the RNeasy Mini Kit (QIAGEN Inc., Valencia, CA), according to the manufacturer's instructions.

Hormone measurements

Serum LH concentrations were measured using an immunofluorometric assay (Delfia, Wallac Oy, Turku, Finland) as described previously (19). Corticosterone concentrations were measured using an RIA (MP Biomedicals, LLC, Orangeburg, NY; ref. 07-120102). Prolactin concentrations were measured by RIA as described earlier (20). Estradiol concentrations were measured using fluoroimmunoassay (Delfia). All hormonal assays were performed from each of the animal groups, as mentioned in the *Results* (n = 8–13 animals per group), 6 months after Ovx.

Adrenocortical tumor assessment

Because the affected animals show bilateral neoplasias, only monolateral evaluation of the tumors was performed. After killing, the adrenal glands were dissected out and fixed in formalin overnight. Tissues were dehydrated in ethanol and left in Histoclear buffer overnight. Adrenals were paraffin embedded, sectioned at 6 μm thickness, and then stained with hematoxylin-eosin according to standard protocols. Eight to 10 slides of five sections were generated for each gland and screened for complete evaluation. The adrenal TS was confirmed when concomitant presence of B cells within foci of A cell expansions were found to disturb the normal architecture of the cortex.

Alternatively, for linkage study, TS was staged. Stage 1 indicated a normal gland as it appears in non-Ovx CTL. Stage 2 designated presence of subcapsular foci of cell proliferation with no abnormal proliferation yet. Glands classified within stages 1 and 2 were considered as nontumorous. Stage 3 showed B cells associated with A cell expansion in the inner part of the cortex. Stage 4 indicated well-established tumor with total cortical disorganization. Glands classified within stages 3 and 4 were considered as tumorigenic.

Inheritance of the traits

Weight gain (WG) was followed up to 6 months after Ovx in F1 (n = 46), DBA/2J (n = 25), C57BL/6J (n = 24), and non-Ovx animals (n = 10–14). TS was assessed at 6 months after Ovx in the same groups (except n = 20 in Ovx-F1).

Immunohistochemistry

Paraffin-embedded tissue sections were deparaffinized, hydrated, and boiled in 10 m$_M$ citric acid (pH 6.0) for antigen retrieval. Three percent H$_2$O$_2$ in PBS was used to block endogenous peroxidases, after which the slides were incubated with 1.5% normal serum in PBS. Sections were stained with primary polyclonal goat antimouse LHR M-17 antibody or primary polyclonal goat antihuman FRP-1 C-19 antibody (sc-26434 and sc-7425, respectively; Santa Cruz Biotechnology, Santa Cruz, CA) at dilution 1:100 for 1 h at room temperature. The avidinbiotin immunoperoxidase system was used to visualize bound antibody (Vectastain Elite ABC kit; Vector Laboratories, Burlingame, CA) with diaminobenzidine substrate kit (SK-4100; Vector). Slides were then counterstained with hematoxylin.

Laser capture microdissection of adrenal cortex

Adrenal glands were embedded in Tissue-Tek (Miles, Elkhart, IN) and frozen in liquid nitrogen. Cryosections (10 μm thick) were cut and mounted onto ribonuclease-treated membrane slides (PALM Microlaser Technologies AG, Bernried, Germany). Sections were fixed (3 min) in 65% ethanol, counterstained briefly (5–10 sec) with hematoxylin-eosin, and dehydrated in 100% ethanol. Neoplastic area and normal adjacent cortex area were isolated from these sections using the PALM Robot-Microbeam version 4.0 (PALM Microlaser Technologies). Laser capture was performed with an approximately 15- to 30-μm laser beam, a laser power of 50 mV, and a laser power duration of 4–6 msec. Cells were collected in PALM AdhesiveCaps tubes that were stored on dry ice until RNA extraction. RNA was extracted within 2 h of cell collection using the RNeasy Micro Kit (QIAGEN), according to the manufacturer's instructions. All RNA extracted was used for the RT reaction (Invitrogen Life Technologies, Inc., Paisley, UK) as described below.

RT-PCR

One microgram of total RNA was reverse-transcribed using the SuperScript First-Strand Synthesis System for RT-PCR (Invitrogen Ltd., Paisley, UK), according to the manufacturer's instructions. The resulting first-strand cDNA was used as a template in subsequent PCR. Sense and antisense primers for *LHR* and *L19 ribosomal protein* internal control were designed as previously described (15). PCR conditions for *LHR* were as follow: 94 C for 1 min, 53 C for 1 min, and 72 C for 1 min for 29 cycles. Same PCR conditions were used for *L19* except 27 cycles and annealing temperature of 60 C. The sense primer for *Sfrp1* was 5′-TGCTCAAATGTGACAAGTTC-3′, and the antisense primer was 5′-CGTGGTTTTTCATTCTCTTC-3′. PCR conditions for *Sfrp1* were 94 C for 1 min, 47 C for 1 min, and 72 C for 1 min for 30 cycles.

Then, PCR products were loaded on 2% agarose gel containing ethidium bromide to identify the amplicons. Densitometric analysis was performed with the Image J software (Image J 1.36b; Wayne Rasband, National Institutes of Health, Bethesda, MD), and gene expression was normalized to *L19* expression. Results for *LHR* are expressed as fold induction *vs.* the background signal measured in non-Ovx control samples, and results for *Sfrp1* are expressed as percentage of expression *vs.* expression in normal tissue.

Statistical analysis

The data presented are expressed as mean $\pm$ SD, with the minimum number of samples being five per group. Statistically significant differences were determined by nonparametric *t* test (Mann Whitney *U* test) or by χ^2 goodness-of-fit test (with one degree of freedom; critical value = 3.8); $P < 0.05$ was considered statistically significant.

Genome-wide scan

Genomic DNA was isolated from liver tissue, purified, and quantified according to standard protocols.

Using the Mouse Phenome Database (http://www.jax.org/phenome/snp.html) and the NCBI Database (build 36.1), 192 informative single-nucleotide polymorphisms (SNPs) that distinguish the two parental strains (*i.e.* DBA/2J and C57BL/6J) were selected at about 10-cM intervals across the mouse genome, and not more than 5 cM from the chromosome ends. The average spacing between SNPs was 7.7 cM ($\pm$ 4.5 cM), the largest gap between two SNPs being 20 cM.

SNP assays were performed using the SEQUENOM MassARRAY system. Briefly, primers for PCR and single-base extension were designed by using the MassARRAY Assay Design 3.1 software package (SEQUENOM, Hamburg, Germany), and SNPs were multiplexed into a maximum of 36-plex pools by using the software. SNP amplification and iPLEX reaction were carried out according to the iPLEX Gold application guide. Completed genotyping reactions were spotted in nanoliter volumes onto a matrix arrayed into 384 elements on a silicon chip (SEQUENOM SpectroCHIP), and the allele-specific mass of the extension product was determined by matrix-assisted laser desorption ionization/time-of-flight mass spectrometry. Analysis of data by MassARRAY Typer 3.4 software for iPLEX generates automated allele calling. Plates were considered successful if more than 75% of genotypes could be called and there was no significant deviation from Hardy-Weinberg equilibrium ($P > 0.05$).

Linkage analysis

The genetic map in both F2 and BC crosses was estimated from the data using the Lander-Green algorithm (21), and genotyping errors were identified by calculating the error LOD for each genotype as described by Lincoln and Lander (22).

We carried out genome-wide linkage analysis to identify genomic regions associated with TS and WG using the R/qtl package (23) in the F2 (n = 208) and BC (n = 125) populations. We used a two-step approach by first identifying the regions of interest showing nominal evidence for linkage (two-point LOD scores > 3) and then refining the QTL mapping by adding additional SNPs. LOD scores were computed at 1-cM intervals, and empirical genome-wide significance was calculated by 10,000 permutations (24).

Two regions were followed up in the second stage: on chromosome 7 and chromosome 8 (average marker density, two per Mbp) for WG and TS, respectively. The 1-LOD drop interval was used as an estimate for the 90% confidence interval of the QTL (25) and was defined after additional SNPs had been added in the region to obtain the highest information content. For the genome-scans of both TS (staged from 1–4) and WG, a nonparametric model was used, which is an extension of the Kruskal-Wallis test (23), allowing robust mapping of QTL without concern about the precise distribution of the trait (26).

For the binary TS (affected/nonaffected), we implemented the binary model (27) using the Haley-Knott regression method (28). To evaluate the effect of obesity, we reanalyzed the tumorigenesis trait fitting two separate models using WG as a covariate (model 1) and using WG as a covariate interacting with QTL genotype (model 2) (29). The difference in LOD scores between the standard model and either model 1 or model 2 was calculated and used to estimate the magnitude of QTL × obesity interaction. A difference of at least 1 LOD between models was considered indicative of the QTL being affected by the obesity covariate.

Two-dimensional genome scan with a two-QTL model was carried out using the R/qtl package (23) and the binary model for TS was implemented; empirical significance of the joint LOD score was assessed by 1000 permutations.

Identical by descent (IBD) analysis

Predicted IBD blocks of shared ancestry for chromosome 8 were estimated between C57BL/ 6J and DBA/2J using the Scripps Florida Mouse Database, 20k dataset (30). Block positions were based on raw SNPs.

Results

Adrenal gland tumor development

In a preliminary experiment, prepubertal Ovx induced adrenocortical neoplasms in DBA/2J mice (n = 13; Fig. 1A) at 6 months after surgery, with 100% penetrance, as reported before (16). Nonsusceptible C57BL/6J mice (n = 11) never developed tumors after Ovx and retained the normal zonal cortical organization (Fig. 1B). In an advanced tumor, spindle-shaped A cells extended from zona glomerulosa to zona fasciculata, whereas lipid-laden B cells were clearly visible between the tracts of A cells (Fig. 1C). As a result, a clear tumorigenic pattern was observed in these glands with complete zonal disorganization of the adrenal cortex. The histological appearance of tumors was similar in F1 (n = 20; Fig. 1C), BC (data not shown), and F2 animals (Fig. 1D), suggesting the same tumorigenic event in all crosses.

Hormonal changes and adrenal LHR expression in Ovx animals

In keeping with a previous report (14), we observed a gonadectomy-induced increase in serum LH levels (20- to 27-fold) that was similar in both parental strains when compared with non-Ovx controls (n = 11–13 per group; Fig. 2A, *inset*). Similar patterns of LH levels were observed in the F2 cross and BC mice (n = 8–13 per group; Fig. 2A), but the increases were not correlated with WG or TS ($P > 0.1$).

Because the DBA/2J mice also developed massive obesity paralleling tumor growth, serum corticosterone concentrations were assessed in the same animal groups. Gonadectomy did not affect corticosterone levels in either the parental strains or crosses (Fig. 2B), and corticosterone levels were not correlated with either WG or TS ($P > 0.1$). No tumor- or Ovx-related changes in serum estrogen or prolactin levels were observed (data not shown).

RT-PCR analysis on adrenal gland extracts of gonadectomized mice showed clear LHR mRNA expression and a clear increase in expression from 3 months after the surgery was observed in F1, DBA/2J, and in nonsusceptible C57BL/6J strains (n = 3–5 per group; Fig. 3A), compared with non-Ovx animals where the LHR gene cannot be detected. Expression after 6 months was similar in all animals including the F2 population (Fig. 3A).

LHR expression was confirmed by immunohistochemistry (Fig. 3B). The wild-type adrenals were immunonegative, whereas clear staining was observed within the tumors (Fig. 3B, Ovx-F1). The cortical region also displayed clear staining in Ovx-C57BL/6J mice, indicating that nontumorigenic adrenal glands also express LHR ectopically after gonadectomy (Fig. 3B). Altogether, these results confirm that LHR expression is undetectable in the normal adult adrenal gland, whereas it becomes ectopically expressed and is clearly up-regulated after Ovx.

Inheritance and segregation of the tumorigenic and obesity traits

All Ovx-F1 mice displayed significant WG from 2 months after surgery, suggesting a dominant mode of inheritance for this trait (n = 10–46; Fig. 4). Similarly, all Ovx-F1 mice developed

adrenocortical tumor (as shown in Fig. 1C; n = 20), which is suggestive of a dominant mode of inheritance also for TS.

Staging of the tumors (see *Materials and Methods*) revealed that 70.1% of F2 and 56.8% of BC adrenal glands were tumorigenic (Fig. 5A). These ratios were not different from those expected in the case of a monogenic inheritance ($\chi^2 = 0.14$; $P > 0.05$), suggestive of genetic control by a single gene.

The estimated heritability for WG was 58%, indicating a substantial genetic component segregating in the F2 population for this trait. We did not observe a significant difference ($P = 0.8$) in the distribution of WG for the F2 and BC populations at month 6 (17.8 ± 5 g in F2 and 17.6 ± 4 g in BC; mean $\pm$ sd; Fig. 5B), and the Castle-Wright estimation (31) indicated a minimum of two segregating genes, suggestive of a polygenic control of WG. Although WG coincides with adrenal tumorigenesis in DBA/2J, we did not observe a significant correlation ($P > 0.5$) between WG and TS in either F2 or BC mice (Fig. 5C).

Although both WG and TS were gonadectomy induced, we concluded that TS is under a different genetic control than WG, and accordingly, we analyzed these traits separately.

Linkage analysis

We detected significant linkage for WG on chromosome 7 (Fig. 6A), with a LOD score of 4.79 ($P = 0.01$) in the F2 population. Interval mapping indicated a broad region spanning about 30 cM, between SNPs rs13479333 and rs4226783 (Fig. 6B). No nominal evidence for linkage at this locus (LOD < 1) was observed in the BC population. Other suggestive linkages in the F2 were observed on chromosomes 11 (LOD = 2.84), 1 (LOD = 2.65), 5 (LOD = 2.2), 14 (LOD = 2.17), and 3 (LOD = 2.14).

Using a nonparametric model for staged TS in the F2 cross, we found only one highly significant linkage, with a LOD of 5.57 ($P = 0.001$) for tumorigenesis (Fig. 6C). Interval mapping indicated a broad peak spanning about 35 cM on chromosome 8, with a 1-LOD drop from the maximum peak height defining an interval of about 10 cM located between markers rs32607714 and rs6382288 (Fig. 6D). One other suggestive linkage was observed on chromosome 10 (LOD = 2.2), but did not reach significance. No significant linkages were detected in the BC population for TS, although the highest LOD (1.5) was observed at the same locus (data not shown).

When TS was analyzed as a dichotomous trait (tumor/normal), the same QTL on chromosome 8 (LOD = 4.0; $P = 0.05$) was observed. Models with WG as a covariate and as a covariate interacting with the QTL on chromosome 8 (see *Materials and Methods*) did not show a significant change in the LOD score for TS (maximum change in LOD score < 0.2 in both models), suggesting a lack of interaction between the TS locus and WG.

Two-dimensional genome scan for TS

Analysis of the segregating alleles within the TS QTL at SNP rs33209429 (peak of linkage) revealed that 27.9% of the tumorigenic F2 animals were homozygous for the nonsusceptible C57BL/6J allele, and 40% of the nonaffected F2 animals were homozygous for the susceptible DBA/2J allele.

Although the TS segregation pattern in the F2 was consistent with a dominant, monogenic model of inheritance, the underlying genetic architecture appeared to be more complex and likely to involve a polygenic component. Therefore, we carried out a two-dimensional genome scan for TS and tested for genome-wide QTL-QTL interaction. The only significant interaction was obtained for two loci on chromosomes 8 and 18 (joint LOD = 8.32; $P < 0.05$, Fig. 7 and

Table 1). Although the locus on chromosome 18 did not show significant linkage in the single-locus genome scan, it appeared to contribute to TS under a two-locus model of epistasis. This suggests that the main susceptibility locus on chromosome 8 is likely to be modulated by a secondary QTL on chromosome 18. We investigated the QTL region on chromosome 18 (spanning 10 Mbp between positions 80 and 90 Mbp), which includes 62 annotated genes, but did not find any genes with obvious functional relevance to tumorigenesis.

Identification of candidate genes for TS

The TS QTL on chromosome 8 spanning a 10-cM interval contains 123 genes (according to the NCBI genome viewer, build 36.1). Among those, 34 unknown/similar/hypothetical genes and 42 belonging to the defensin-related cluster of genes were not prioritized as candidates for TS.

Using IBD analysis, we excluded blocks of shared ancestry between both parental strains (see supplemental data, published on The Endocrine Society's Journals Online web site at http://endo.endojournals.org) and further refined the number of potential candidates to 34. Thirty-one genes have human orthologs (Table 2), with their functions being related to transport, transcription, proteolysis, cell cycle, metabolism, cell adhesion, and negative regulation of the Wnt signaling pathway.

We focused on the nine genes that showed sequence variation in the coding region between the parental strains, according to the Mouse Phenome Database and the NCBI database. Among these genes, none have previously been reported to be expressed in the mouse adrenal gland (databases: Unigene-ensembl, NCBI). Furthermore, we confirmed the absence of mRNA expression in the adrenal gland for all but one of the candidate genes in the list, including *Dkk4, Zmat4, Slc20a2, Adam9, Adam18, Tpte, Mcph1*, and *Defensin-β1* (data not shown). On the other hand, we could detect *Sfrp1* (secreted frizzled-related protein 1) mRNA expression in adrenal gland extracts. As shown in Fig. 8A, *Sfrp1* transcripts were found in normal and tumorigenic adrenal samples from whole glands and enriched tumorigenic areas (isolated by laser capture microdissection), respectively (Fig. 8A), which prompted us to examine further this gene.

The *Sfrp1* tumor suppressor gene is an attractive positional candidate because it is involved in the Wnt pathway, which has previously been suggested in adrenocortical tumorigenesis in mice (13). We sequenced all the nonsynonymous coding variants reported between the two parental strains for *Sfrp1,* as well as for each of the candidate genes where such variants have been reported, but we could not find any evidence for associations with the TS phenotype (data not shown). The putative promoter region of *Sfrp1* was also screened for possible variants between the two parental strains, but no SNPs were found. Alternatively, *Sfrp1* expression in the adrenocortical tumors was assessed by immunohistochemistry, and we showed that the neoplastic regions exhibited less intense staining for the protein compared with adjacent normal cortex (Fig. 8B, a–c). In particular, Sfrp1 staining was absent in the neoplastic A cells (Fig. 8B, d), suggesting that the absence or lower level of expression of this tumor suppressor gene product could contribute to the initiation of tumor development. In early stages of TS (third month after Ovx, Fig. 8B, e), characterized by A cell proliferation and zonal invasion, Sfrp1 protein was not detected in A cells compared with the adjacent normal cortex. Normal adrenal cortex from nontumorigenic glands of Ovx-C57BL/6J mice showed regular Sfrp1 staining (Fig. 8B, f).

Discussion

We report here the first study on the genetic basis of LH-induced adrenocortical neoplasia in nonsusceptible C57BL/6J and susceptible DBA/2J inbred strains of mice. These strains

represent a unique physiological model that may have relevance for the pathogenesis of postmenopausal adrenal tumors in humans. Women are exposed to high levels of LH for years after menopause, and LH-stimulated adrenal function is a plausible hypothesis for the increased occurrence of postmenopausal adrenal tumors and obesity. Moreover, aberrant LHR expression has been reported in patients developing macronodular adrenal hyperplasia associated with Cushing's syndrome (8).

Several studies on different mouse models developed by us and others have shown that there are more than one tumor type that are induced by high LH in mouse adrenal glands (10), with some arising from different zones of the gland such as the X zone (32) or the subcapsular cortical zone. Interestingly, the adrenocortical tumors presented in the postgonadectomy mouse model resemble closer luteal cell rests rather than adrenal tumors, as suggested in early work of Fekete *et al.* (16). This is in accordance with our observation that these tumors do not secrete corticosterone (Fig. 2B) and show clear expression of steroidogenic differentiation markers and GATA-4 in the tumorigenic cortex, as reported in several studies (13-15).

Recent reports emphasize that inappropriate adrenocortical expression of nonmutated G protein-coupled receptors, such as LHR or gastric inhibitory peptide receptor, is sufficient to induce tumor formation (33,34). However, our data show that the ectopic LHR expression in the adrenal cortex is not a sufficient causative event for neoplasia because also the nonsusceptible C57BL/6J mice expressed LHR in the adrenal gland after Ovx, without development of tumors (Fig. 3). Moreover, the switch from the predominantly adrenal expression of transcription factor GATA-6 to expression of the gonad-specific GATA-4 has been reported in a subset of human and mouse adrenocortical tumors (14,35), which can amplify the adrenal overexpression of LHR (15). We detected *GATA-4* mRNA in normal adrenals of Ovx mice (data not shown), suggesting that unknown factor(s) other than LH/LHR/GATA-4 might be involved in the etiology of the tumor phenotype.

Genetic predisposition to tumorigenesis in the adrenal gland has been inferred (36), and high LH levels have been proposed as the trigger, to induce ectopic LHR expression in adrenal glands (14). Although LH rise is the prerequisite for the induction of tumorigenesis in DBA/2J animals, we showed that the TS is not the obligate consequence of high LH and adrenal LHR overexpression (Figs. 2 and 3) because nontumorigenic Ovx-C57BL/6J animals exhibit similar LH levels and LHR overexpression. This finding suggests that different genetic backgrounds influencing the downstream events from LHR activation contribute to the induction of the neoplastic phenotype. We therefore carried out a genome-wide search to identify genetic factors associated with post-gonadectomy adrenocortical tumors in mice.

Linkage analysis identified a major locus on chromosome 8 in F2, although we did not observe significance in the BC population. This lack of replication may be due to the lower power of QTL detection by linkage in the BC compared with the F2 population (31). No evidence for linkage to *LHR* (chromosome 17) and *GATA-4* (chromosome 14) genes was found, excluding them as candidates for tumorigenesis. We propose this locus on chromosome 8 as a new locus involved in mouse adrenocortical tumorigenesis. One study exists on mapping mouse adrenocortical dysplasia to the central region of chromosome 8 (37,38), at a close but distinct genomic region. This is of potential interest because cortical cells of the affected adrenocortical dysplasia mice contained lipid droplets characteristic of steroidogenic cells, which resembles those of B cells in our phenotype. Interestingly, allelic imbalance of human chromosome 8p (syntenic region to our locus) has been described in many human cancers (39), supporting the hypothesis that genes in this region play an important role in human tumorigenesis, but none have been reported for mouse adrenal tumors.

A separate QTL linked to WG was identified on chromosome 7, suggesting that postgonadectomy obesity and adrenal tumorigenesis are segregating independently. This is in accordance with the unchanged corticosterone levels we measured in the animals after Ovx (Fig. 2B), suggesting other genetic factors contributing to WG in this model. In accordance, previous studies have identified several QTL for obesity on mouse chromosome 7 in several mouse models (40-42), providing strong evidence that the WG in our model is an independent obese phenotype from the adrenal condition.

We identified a highly significant susceptibility locus for adrenal gland tumorigenesis in DBA/2J mice on chromosome 8. Unexpectedly, we found a significant proportion of unaffected F2 animals carrying the susceptible DBA/2J alleles at this locus. This inverse association of the risk allele with the phenotype has been reported in humans (flip-flop phenomenon) (43) and is usually attributable to hidden genetic heterogeneity due to sampling effects. It was hypothesized that flip-flop associations may be attributable to undetected multilocus effects or to noncausal variant in linkage disequilibrium with the genuine causal variant (43). Although the observed negative association could indicate the presence of a protective allele at the locus of interest, we hypothesized the presence of a polygenic component interacting with the major QTL for TS.

We therefore carried out a genome-wide epistasis analysis and showed that the major QTL for TS is significantly modulated by at least one other locus, on chromosome 18. When the combined effect of the genotypes at both chromosome 8 and 18 loci was investigated, we observed the resistant C57BL/6J allele in about 20% of tumorigenic F2 animals, suggesting the presence of undetected loci of small effect. Epistasis analysis showed that 10 of 12 nonsignificant interactions (Table 1) involved the locus on chromosome 8, supporting the hypothesis of multiple interacting loci contributing to the phenotype.

The major QTL identified on chromosome 8 spans an approximately 10-cM region, containing 31 candidate genes, orthologs to human, none of them previously identified to interact with LHR function. Among these genes, *Sfrp1* is an attractive positional candidate because it is a dominant-negative inhibitor of the Wnt signaling pathway (44), which contributes to tumorigenesis when dysregulated (45).

Sfrp1 is down-regulated by epigenetic modifications in several types of cancers, indicating a putative tumor suppressor role for this gene (46,47). We have not excluded epigenesis as a mode of action of this gene in our model, because we screened only the coding region, but to our knowledge, no data have been reported that support epigenetic changes of *Sfrp1* in a tumorigenic mouse model. Bielinska *et al.* (13) reported in adrenal gland tumors from NU/J mice a possible role for the Wnt signaling pathway in the pathogenesis, which prompted us to test for *Sfrp1* expression in our model. We found that normal adrenal glands do express *Sfrp1*, as shown in C57BL/6J, whereas the expression is strongly altered in adrenocortical tumors. Thus, subcapsular A cells, *i.e.* the first stage of adrenal tumors, do not seem to express this gene, whereas cortical B cells do.

This observation may be of significance because it was recently suggested that adrenocortical tumors from Ovx-CE/J mice are derivatives from cells of the proposed subcapsular stem cell zone (48). In addition, there is evidence for a pool of stem or progenitor cells that reside in this subcapsular cellular compartment, likely to play a key role in adrenal physiology as the origin of all adrenocortical cells that migrate centripetally upon differentiation (49,50). These adrenocortical stem cells remain pluripotent and can adopt a gonadal fate, as a reminiscence of the adrenogonadal primordium during embryonic development. Then, when gonadotropin levels are disproportionately high, as after Ovx, the stem cells could give rise to tumors that resemble functional gonadal cells, as observed in adrenocortical tumorigenesis. It is not known

whether A cells are the stem cells, but because they both originate from the same zone, the tumorigenesis observed could be an example of stem cell metaplasia. It was recently shown that a subset of subcapsular adrenocortical cells retain the developmental plasticity to respond to pituitary gonadotropic stimuli and that these cells become dysregulated due to convergent Ovx and chronic LH exposure, thus leading to hyperproliferative clusters of cells in the adrenal cortex culminating in tumorigenesis (51).

It is noticeable that although *Sfrp1* is an attractive candidate within the locus on chromosome 8, based on location, biology, and protein expression, we cannot exclude any of the other genes within this interval. Although we did not detect gene expression for the other candidate genes, such as *Dkk4* (which is also involved in the Wnt signaling pathway), it is possible that these genes are expressed at very low or undetectable levels. It is also possible that the genes of interest reside in the region of IBD and had a recent mutation in one of the parental strains. Finally, we cannot rule out that other undetected epistatic loci of small contribution, involving other unknown candidate genes, are implicated in the regulation of the phenotype, which brings another level of complexity to the disease. However, *Sfrp1* remains a potential candidate according to its differential expression within the adrenal gland tumor.

In conclusion, this is the first genetic study on LH-induced adrenocortical tumorigenesis in inbred mice. We identified a major, obesity-independent QTL for TS on chromosome 8, which is modulated via epistasis by another QTL on chromosome 18, revealing a complex genetic architecture. We propose adrenal tumorigenesis in DBA/2J mice as a model of adrenal stem cell dysregulation, relayed by Wnt signaling (52). We identified the *Sfrp1* tumor suppressor underlying the major QTL for TS as an attractive candidate for adrenal tumorigenesis, although more studies are needed to confirm its role in the pathogenesis of the disease as well as to find other associated genes.

Acknowledgments

Abbreviations

BC, Backcross; IBD, identical by descent; LHR, LH receptor; Ovx, ovariectomized; QTL, quantitative trait loci; Sfrp1, secreted frizzled-related protein 1; SNP, single-nucleotide polymorphism; TS, tumor status; WG, weight gain.

References

1. Mantero F, Terzolo M, Arnaldi G, Osella G, Masini AM, Ali A, Giovagnetti M, Opocher G, Angeli A. A survey on adrenal incidentaloma in Italy. Study Group on Adrenal Tumors of the Italian Society of Endocrinology. J Clin Endocrinol Metab 2000;85:637–644. [PubMed: 10690869]

2. Thompson GB, Young WF Jr. Adrenal incidentaloma. Curr Opin Oncol 2003;15:84–90. [PubMed: 12490767]

3. Fidler WJ. Ovarian thecal metaplasia in adrenal glands. Am J Clin Pathol 1977;67:318–323. [PubMed: 851092]

4. Givens JR, Andersen RN, Wiser WL, Coleman SA, Fish SA. A gonadotropin-responsive adrenocortical adenoma. J Clin Endocrinol Metab 1974;38:126–133. [PubMed: 4358642]

5. Romberger CF, Wong TW. Thecal metaplasia in the adrenal gland of a man with acquired bilateral testicular atrophy. Arch Pathol Lab Med 1989;113:1071–1075. [PubMed: 2549908]

6. Bertherat J, Mosnier-Pudar H, Bertagna X. Adrenal incidentalomas. Curr Opin Oncol 2002;14:58–63. [PubMed: 11790982]

7. Lacroix A, Baldacchino V, Bourdeau I, Hamet P, Tremblay J. Cushing's syndrome variants secondary to aberrant hormone receptors. Trends Endocrinol Metab 2004;15:375–382. [PubMed: 15380809]

8. Christopoulos S, Bourdeau I, Lacroix A. Clinical and subclinical ACTH-independent macronodular adrenal hyperplasia and aberrant hormone receptors. Horm Res 2005;64:119–131. [PubMed: 16215323]

9. Wy LA, Carlson HE, Kane P, Li X, Lei ZM, Rao CV. Pregnancy-associated Cushing's syndrome secondary to a luteinizing hormone/human chorionic gonadotropin receptor-positive adrenal carcinoma. Gynecol Endocrinol 2002;16:413–417. [PubMed: 12587537]

10. Bielinska M, Kiiveri S, Parviainen H, Männistö S, Heikinheimo M, Wilson DB. Gonadectomy-induced adrenocortical neoplasia in the domestic ferret (*Mustela putorius furo*) and laboratory mouse. Vet Pathol 2006;43:97–117. [PubMed: 16537928]

11. Kananen K, Markkula M, Mikola M, Rainio EM, McNeilly A, Huhtaniemi I. Gonadectomy permits adrenocortical tumorigenesis in mice transgenic for the mouse inhibin α-subunit promoter/simian virus 40 T-antigen fusion gene: evidence for negative autoregulation of the inhibin α-subunit gene. Mol Endocrinol 1996;10:1667–1677. [PubMed: 8961275]

12. Kero J, Poutanen M, Zhang FP, Rahman N, McNicol AM, Nilson JH, Keri RA, Huhtaniemi IT. Elevated luteinizing hormone induces expression of its receptor and promotes steroidogenesis in the adrenal cortex. J Clin Invest 2000;105:633–641. [PubMed: 10712435]

13. Bielinska M, Genova E, Boime I, Parviainen H, Kiiveri S, Leppäluoto J, Rahman N, Heikinheimo M, Wilson DB. Gonadotropin-induced adrenocortical neoplasia in NU/J nude mice. Endocrinology 2005;146:3975–3984. [PubMed: 15919738]

14. Bielinska M, Parviainen H, Porter-Tinge SB, Kiiveri S, Genova E, Rahman N, Huhtaniemi IT, Muglia LJ, Heikinheimo M, Wilson DB. Mouse strain susceptibility to gonadectomy-induced adrenocortical tumor formation correlates with the expression of GATA-4 and luteinizing hormone receptor. Endocrinology 2003;144:4123–4133. [PubMed: 12933687]

15. Rahman NA, Kiiveri S, Rivero-Muller A, Levallet J, Vierre S, Kero J, Wilson DB, Heikinheimo M, Huhtaniemi I. Adrenocortical tumorigenesis in transgenic mice expressing the inhibin α-subunit promoter/simian virus 40 T-antigen transgene: relationship between ectopic expression of luteinizing hormone receptor and transcription factor GATA-4. Mol Endocrinol 2004;18:2553–2569. [PubMed: 15256532]

16. Fekete E, Woolley GW, Little CC. Histological changes following ovariectomy in mice. J Exp Med 1941;74:1–8.

17. Woolley GW, Little CC. The incidence of adrenal cortical carcinoma in gonadectomized female mice of the extreme dilution strain. Cancer Res 1945;5:193–202.

18. Krishna Murthy AS, Brezak MA, Baez AG. Postcastrational adrenal tumors in two strains of mice: morphologic, histochemical, and chromatographic studies. J Natl Cancer Inst 1970;45:1211–1222. [PubMed: 5488065]

19. Haavisto AM, Pettersson K, Bergendahl M, Perheentupa A, Roser JF, Huhtaniemi I. A supersensitive immunofluorometric assay for rat luteinizing hormone. Endocrinology 1993;132:1687–1691. [PubMed: 8462469]

20. Bergendahl M, Perheentupa A, Huhtaniemi I. Effect of short-term starvation on reproductive hormone gene expression, secretion and receptor levels in male rats. J Endocrinol 1989;121:409–417. [PubMed: 2547009]

21. Lander ES, Green P. Construction of multilocus genetic linkage maps in humans. Proc Natl Acad Sci USA 1987;84:2363–2367. [PubMed: 3470801]

22. Lincoln SE, Lander ES. Systematic detection of errors in genetic linkage data. Genomics 1992;14:604–610. [PubMed: 1427888]

23. Broman KW, Wu H, Sen S, Churchill GA. R/qtl: QTL mapping in experimental crosses. Bioinformatics 2003;19:889–890. [PubMed: 12724300]

24. Churchill GA, Doerge RW. Empirical threshold values for quantitative trait mapping. Genetics 1994;138:963–971. [PubMed: 7851788]

25. Dupuis J, Siegmund D. Statistical methods for mapping quantitative trait loci from a dense set of markers. Genetics 1999;151:373–386. [PubMed: 9872974]

26. Kruglyak L, Lander ES. A nonparametric approach for mapping quantitative trait loci. Genetics 1995;139:1421–1428. [PubMed: 7768449]

27. Broman KW. Mapping quantitative trait loci in the case of a spike in the phenotype distribution. Genetics 2003;163:1169–1175. [PubMed: 12663553]

28. Haley CS, Knott SA. A simple regression method for mapping quantitative trait loci in line crosses using flanking markers. Heredity 1992;69:315–324. [PubMed: 16718932]

29. Solberg LC, Baum AE, Ahmadiyeh N, Shimomura K, Li R, Turek FW, Churchill GA, Takahashi JS, Redei EE. Sex- and lineage-specific inheritance of depression-like behavior in the rat. Mamm Genome 2004;15:648–662. [PubMed: 15457344]

30. Cervino AC, Gosink M, Fallahi M, Pascal B, Mader C, Tsinoremas NF. A comprehensive mouse IBD database for the efficient localization of quantitative trait loci. Mamm Genome 2006;17:565–574. [PubMed: 16783638]

31. Lynch, M.; Walsh, B. Genetics and analysis of quantitative traits. Sunderland, MA: Sinauer Associates Inc; 1998.

32. Beuschlein F, Looyenga BD, Bleasdale SE, Mutch C, Bavers DL, Parlow AF, Nilson JH, Hammer GD. Activin induces x-zone apoptosis that inhibits luteinizing hormone-dependent adrenocortical tumor formation in inhibin-deficient mice. Mol Cell Biol 2003;23:3951–3964. [PubMed: 12748296]

33. Mazzuco TL, Chabre O, Feige JJ, Thomas M. Aberrant expression of human luteinizing hormone receptor by adrenocortical cells is sufficient to provoke both hyperplasia and Cushing's syndrome features. J Clin Endocrinol Metab 2006;91:196–203. [PubMed: 16249277]

34. Mazzuco TL, Chabre O, Sturm N, Feige JJ, Thomas M. Ectopic expression of the gastric inhibitory polypeptide receptor gene is a sufficient genetic event to induce benign adrenocortical tumor in a xenotransplantation model. Endocrinology 2006;147:782–790. [PubMed: 16254030]

35. Kiiveri S, Liu J, Heikkila P, Arola J, Lehtonen E, Voutilainen R, Heikinheimo M. Transcription factors GATA-4 and GATA-6 in human adrenocortical tumors. Endocr Res 2004;30:919–923. [PubMed: 15666845]

36. Huseby RA, Bittner JJ. Differences in adrenal responsiveness to post-castrational alteration as evidenced by transplanted adrenal tissue. Cancer Res 1951;11:954–961. [PubMed: 14886953]

37. Beamer WG, Sweet HO, Bronson RT, Shire JG, Orth DN, Davisson MT. Adrenocortical dysplasia: a mouse model system for adrenocortical insufficiency. J Endocrinol 1994;141:33–43. [PubMed: 8014601]

38. Keegan CE, Hutz JE, Else T, Adamska M, Shah SP, Kent AE, Howes JM, Beamer WG, Hammer GD. Urogenital and caudal dysgenesis in adrenocortical dysplasia (acd) mice is caused by a splicing mutation in a novel telomeric regulator. Hum Mol Genet 2005;14:113–123. [PubMed: 15537664]

39. French AJ, Petroni G, Thibideau SN, Smolkin M, Bissonette E, Roviello F, Harper JC, Koch BR, Anderson SA, Hebbring SJ, Powell SM. Allelic imbalance of 8p indicates poor survival in gastric cancer. J Mol Diagn 2004;6:243–252. [PubMed: 15269302]

40. Diament AL, Warden CH. Multiple linked mouse chromosome 7 loci influence body fat mass. Int J Obes Relat Metab Disord 2004;28:199–210. [PubMed: 14569280]

41. Taylor BA, Phillips SJ. Obesity QTLs on mouse chromosomes 2 and 17. Genomics 1997;43:249–257. [PubMed: 9268627]

42. Itoi-Babaya M, Ikegami H, Fujisawa T, Ueda H, Nojima K, Babaya N, Kobayashi M, Noso S, Kawaguchi Y, Yamaji K, Shibata M, Ogihara T. Fatty liver and obesity: phenotypically correlated but genetically distinct traits in a mouse model of type 2 diabetes. Diabetologia 2007;50:1641–1648. [PubMed: 17549450]

43. Lin PI, Vance JM, Pericak-Vance MA, Martin ER. No gene is an island: the flip-flop phenomenon. Am J Hum Genet 2007;80:531–538. [PubMed: 17273975]

44. Finch PW, He X, Kelley MJ, Uren A, Schaudies RP, Popescu NC, Rudikoff S, Aaronson SA, Varmus HE, Rubin JS. Purification and molecular cloning of a secreted, Frizzled-related antagonist of Wnt action. Proc Natl Acad Sci USA 1997;94:6770–6775. [PubMed: 9192640]

45. Moon RT, Kohn AD, De Ferrari GV, Kaykas A. WNT and β-catenin signalling: diseases and therapies. Nat Rev Genet 2004;5:691–701. [PubMed: 15372092]

46. Veeck J, Niederacher D, An H, Klopocki E, Wiesmann F, Betz B, Galm O, Camara O, Durst M, Kristiansen G, Huszka C, Knuchel R, Dahl E. Aberrant methylation of the Wnt antagonist SFRP1 in breast cancer is associated with unfavourable prognosis. Oncogene 2006;25:3479–3488. [PubMed: 16449975]

47. Dahl E, Wiesmann F, Woenckhaus M, Stoehr R, Wild PJ, Veeck J, Knuchel R, Klopocki E, Sauter G, Simon R, Wieland WF, Walter B, Denzinger S, Hartmann A, Hammerschmied CG. Frequent loss of SFRP1 expression in multiple human solid tumours: association with aberrant promoter methylation in renal cell carcinoma. Oncogene 2007;26:5680–5691. [PubMed: 17353908]

48. Johnsen IK, Slawik M, Shapiro I, Hartmann MF, Wudy SA, Looyenga BD, Hammer GD, Reincke M, Beuschlein F. Gonadectomy in mice of the inbred strain CE/J induces proliferation of sub-capsular adrenal cells expressing gonadal marker genes. J Endocrinol 2006;190:47–57. [PubMed: 16837610]

49. Zajicek G, Ariel I, Arber N. The streaming adrenal cortex: direct evidence of centripetal migration of adrenocytes by estimation of cell turnover rate. J Endocrinol 1986;111:477–482. [PubMed: 3805971]

50. Kataoka Y, Ikehara Y, Hattori T. Cell proliferation and renewal of mouse adrenal cortex. J Anat 1996;188(Pt 2):375–381. [PubMed: 8621337]

51. Looyenga BD, Hammer GD. Origin and identity of adrenocortical tumors in inhibin knockout mice: implications for cellular plasticity in the adrenal cortex. Mol Endocrinol 2006;20:2848–2863. [PubMed: 16873442]

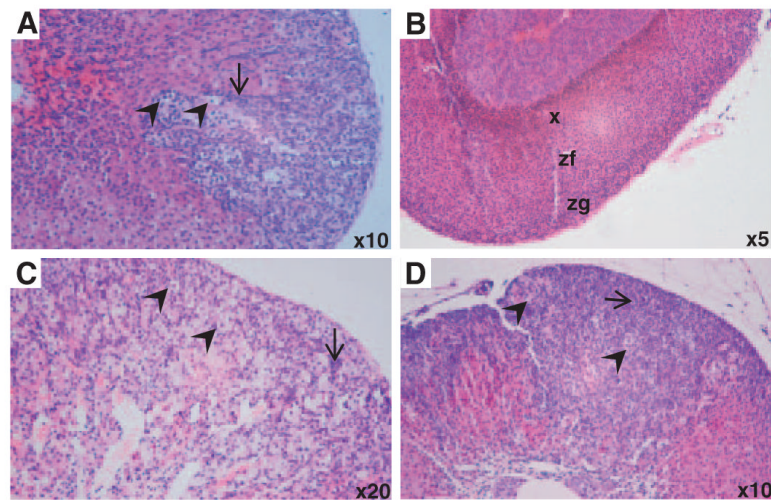52. Nusse R. Wnt signaling in disease and in development. Cell Res 2005;15:28–32. [PubMed: 15686623]

Fig. 1.
Adrenocortical tumor development. A, Adrenal cortex of a prepubertally Ovx-DBA/2J female, 6 months after surgery; B, adrenal gland of an Ovx-C57BL/6J mouse (6 months after surgery) showing normal morphology and normal zonal organization of the cortex, with distinct zona glomerulosa (zg), zona fasciculata (zf), and X zone (x); C and D, tumors from F1 and F2 mice, respectively, showing complete disruption of the zonal organization due to neoplasia. Accumulation of spindle-shaped A cells (*arrows*) and lipid-laden B cells (*arrowheads*) is clearly visible in the cortex as a feature of tumorigenesis. Objective magnification is indicated at the *bottom right corner* of each *panel*.
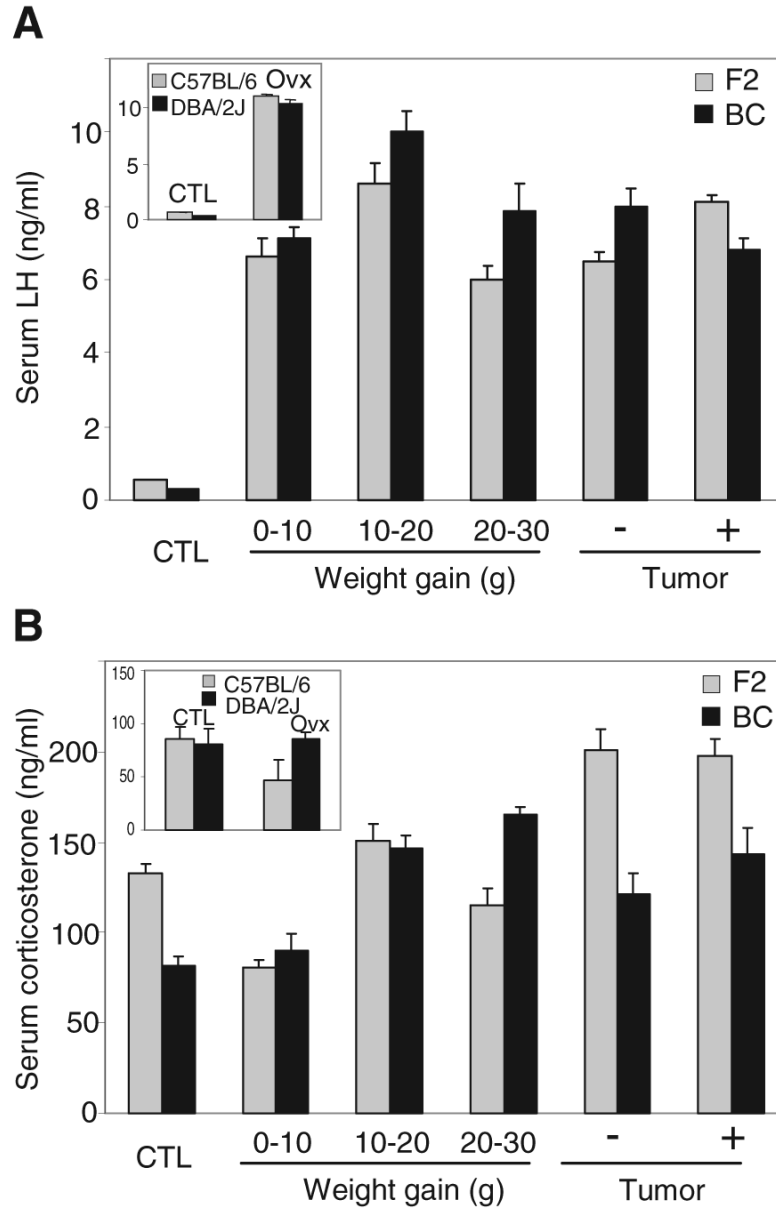
Fig. 2.
Hormone concentrations 6 months after prepubertal Ovx in F2 and BC animals. A, Serum LH. As shown in both parental strains (see *inset*, n = 11–13 animals in each group), Ovx induces high LH levels in F2 (n = 8–13 per group) and BC (n = 8–12 per group) animals, irrespective of their WG and TS. B, Corticosterone levels are not affected by Ovx in the same animal groups. CTL, Control (non-Ovx animals).
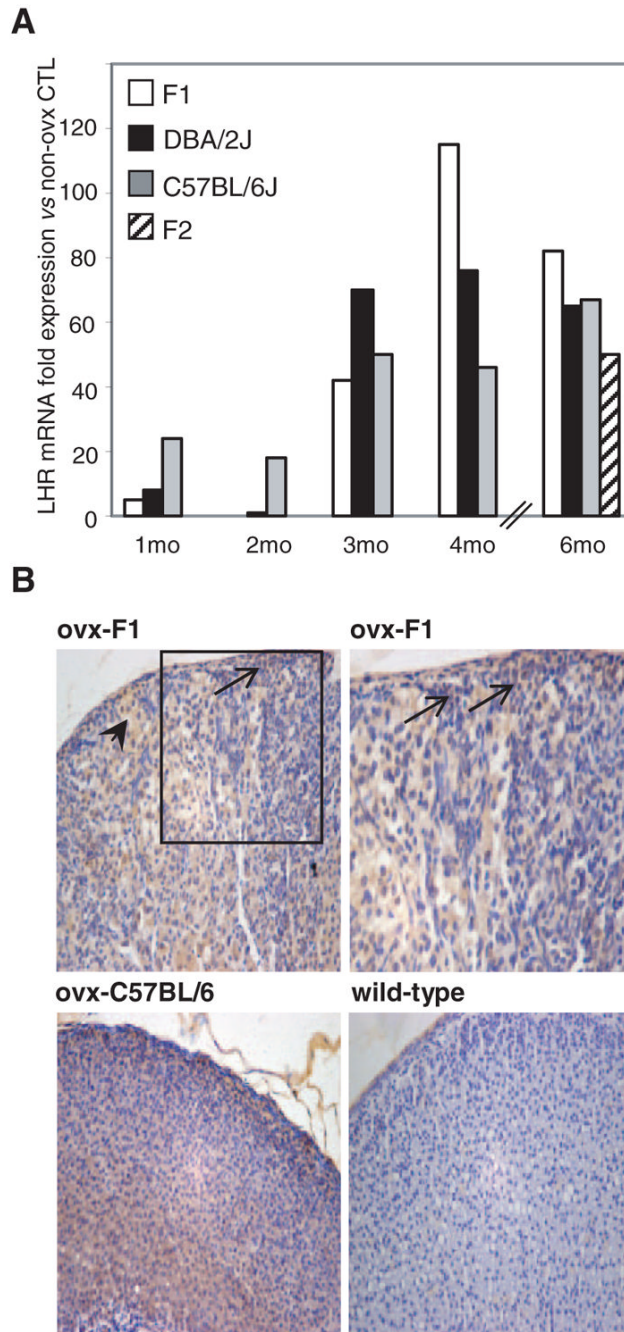
A

B

Fig. 3.
LHR expression in Ovx animals. A, Time course of *LHR* expression was screened up to 6 months after Ovx in parental strains and F1 and F2 progeny. RT-PCR shows *LHR* mRNA expression in adrenal glands of all animal groups (*bars* are means of three to five samples per group). No *LHR* mRNA could be detected in non-Ovx control adrenals. B, Immunohistochemistry with a primary polyclonal anti-LHR antibody showing immunoperoxidase staining in sections from Ovx-F1 and Ovx-C57BL/6J, 6 months after Ovx. The tumorous region is evenly stained in Ovx-F1 within B cells (*arrowheads*) and A cells (*arrows*) as shown in the *two top panels*. The *top right panel* shows a higher magnification of the squared region as indicated in the *top left panel*.
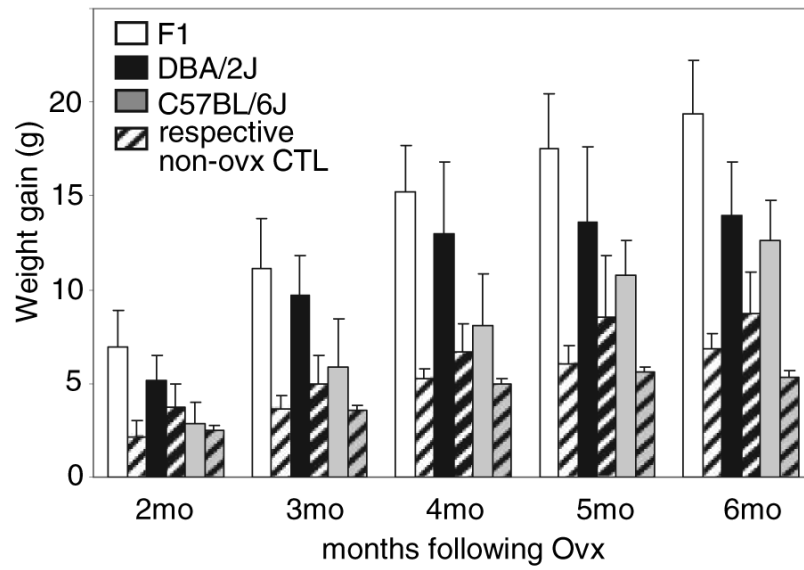
Fig. 4.
Inheritance of the obese phenotype. WG of Ovx C57BL/6J, DBA/2J, and their F1 crosses as well as non-Ovx controls of the same groups (corresponding *hatched bars* of the same *color*) was followed up to 6 months after Ovx (n = 10–46, see *Materials and Methods* for more details).
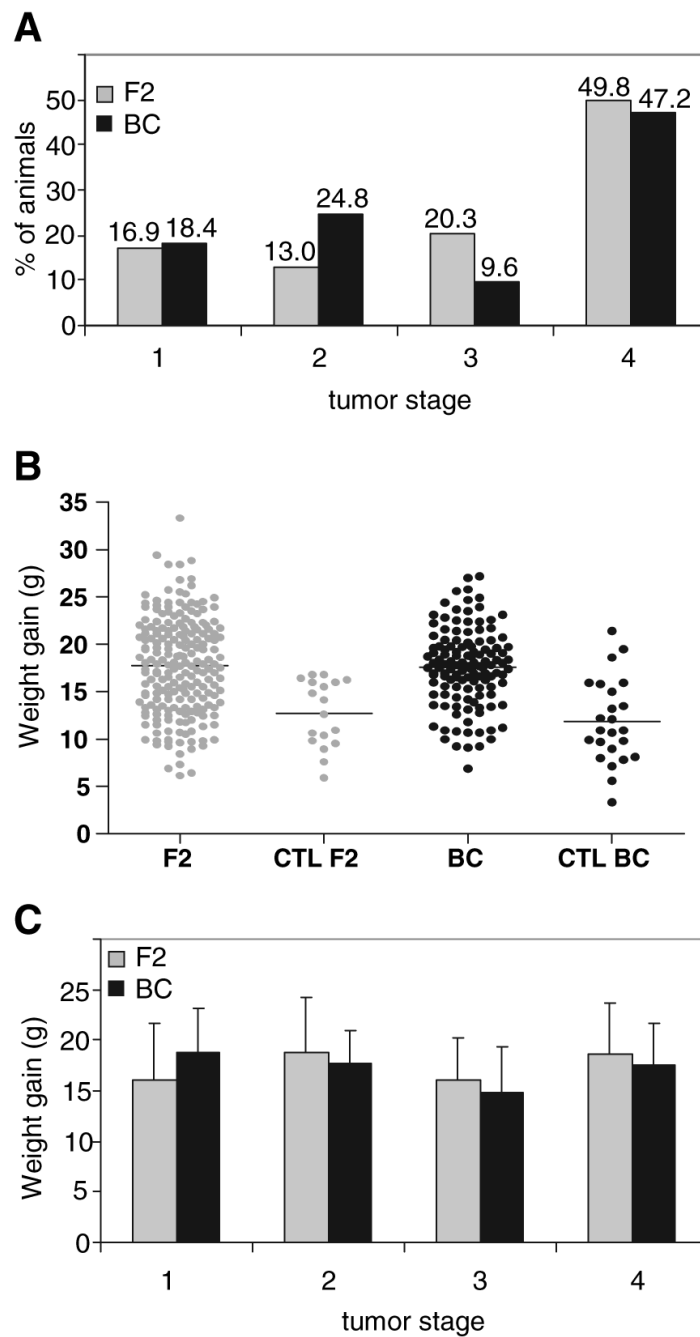
Fig. 5.
Segregation of phenotypes. Penetrance of TS and WG was evaluated in F2 and BC animals. Classification of adrenal gland histology with respect to tumor stage is described in *Materials and Methods*. A, Percentages of F2 and BC mice with each stage of tumor development. B, Distribution of WG in Ovx-F2 (n = 208) and BC (n = 125) animals as well as in their respective non-Ovx controls (CTL; n = 19 –24) is shown. Each dot represents a single animal. C, Correlation between WG and tumor stage in F2 and BC animals. Both groups exhibited similar WG pattern with no effect according to tumor stage.
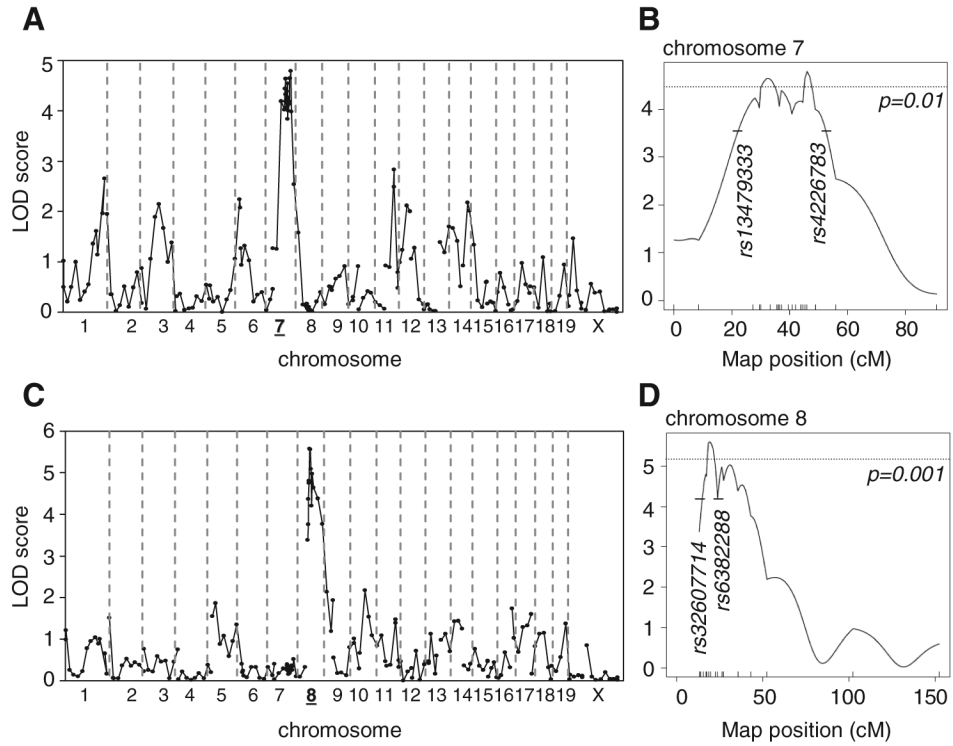
Fig. 6.
Linkage analysis for WG and TS in Ovx-F2 animals. A and C, Genome scans in Ovx-F2 with LOD scores (y-axis) for WG (A) and adrenal gland tumorigenesis (C). Chromosomes are indicated on the x-axis, and LOD scores for each SNP are indicated with *circles* in the graph. B and D, Peaks of linkage at the specified chromosome for WG (B) and tumorigenesis (D), with the distance in centi-Morgans given along the x-axis, and the LOD scores given along the y-axis. *Horizontal thin lines* indicate empirical *P* value thresholds estimated by 10,000 permutations.
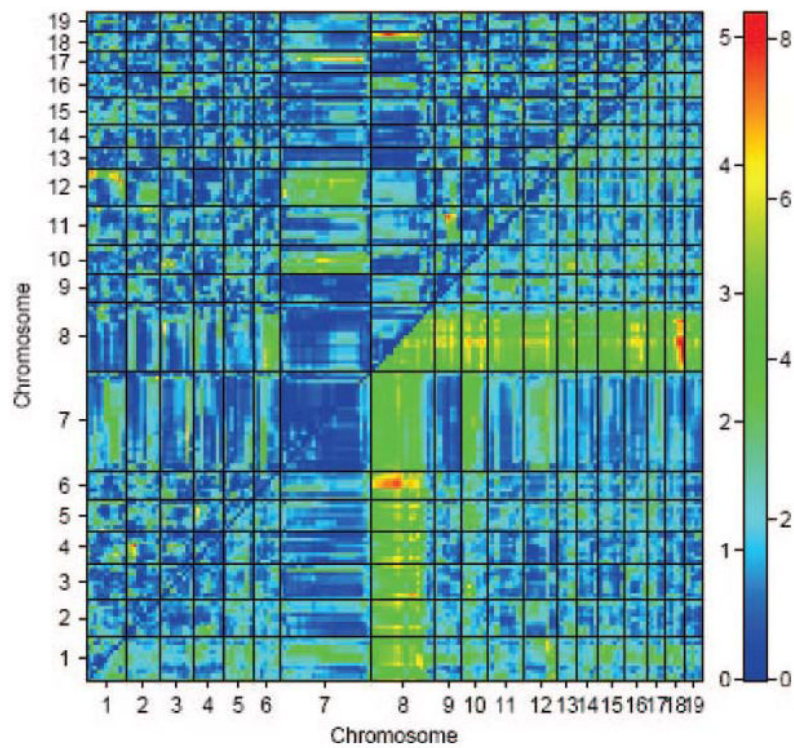
Fig. 7.
F2 two-dimensional genome-wide scan for TS. Epistasis for TS was estimated for each chromosome, as represented along the x- and y-axes, with a two-locus model as described in *Materials and Methods*. *Above the diagonal* are the LOD scores due to the interaction between two QTLs (epistasis), and *below the diagonal* are the LOD scores due to the joint effects of the QTLs. The *color scale* is representing the epistasis (*left*) and the joint LOD scores (*right*).
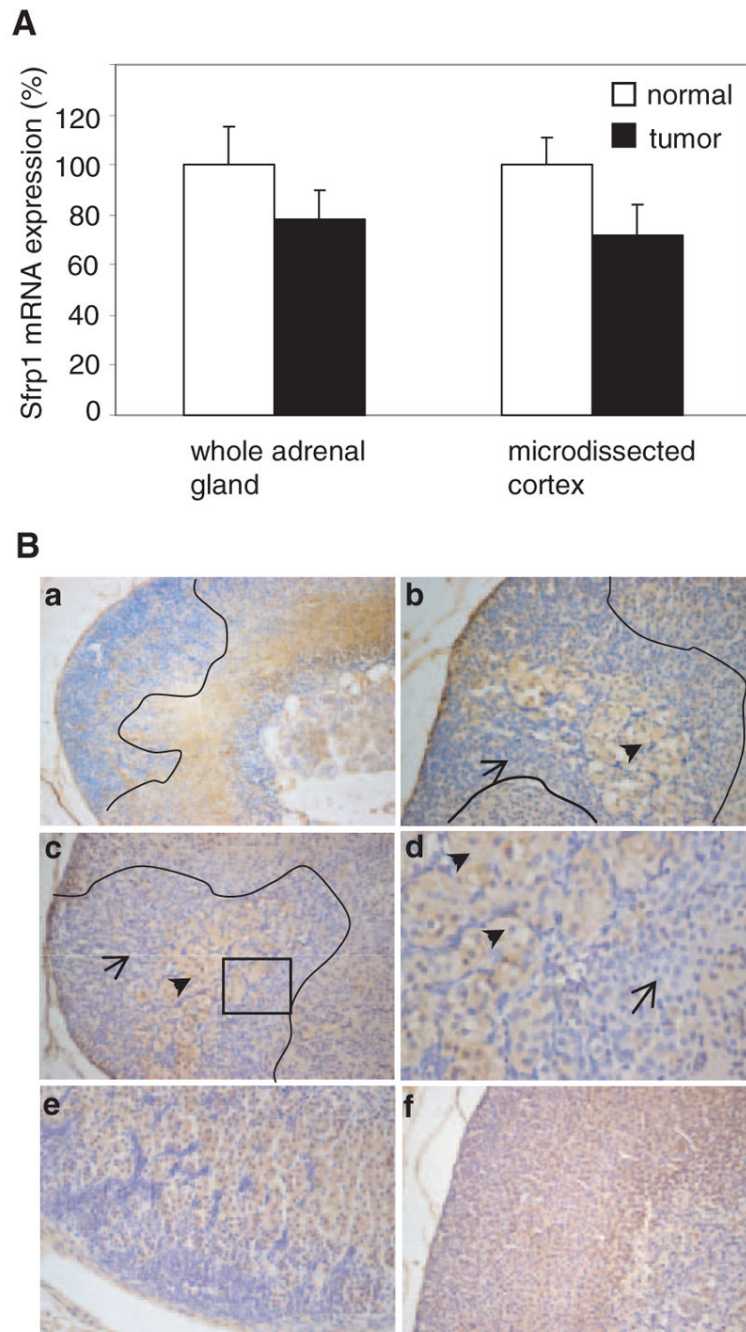
Fig. 8.
Sfrp1 expression in adrenal gland tumors. A, *Sfrp1* mRNA expression in adrenal glands was assessed by RT-PCR from whole normal (n = 5) and tumorigenic (n = 10) adrenal glands (*left bars*) as well from microdissected tumor areas (n = 4) and adjacent normal cortex (n = 4) (*right bars*). Clear expression was observed in normal and tumor tissues, but the levels did not differ significantly. B, Immunohistochemistry with a primary antibody against Sfrp1 was performed on sections from tumorigenic adrenal glands: a, tumorigenic region, delimited by a *black line*, showing less intense staining (*blue area*) of Sfrp1 compared with immunoreactivity of the adjacent normal cortex (*brown* staining); b and c, distinct staining could be seen between A cells (*arrows*; no staining) and B cells (*arrowheads*; staining); d, enlargement of the *boxed*

region in c; e, early stage of tumorigenesis (3 months after Ovx) with clear lack of Sfrp1 expression in invading cells; f, normal cortex of an Ovx-C57BL/6J mouse with uniform staining.

TABLE 1

Maximum LOD scores for the two-dimensional scan for TS in the F2 population

Locus	pos1	pos2	LODjnt	−logP	LODint	−logP	LODq1	−logP	LODq2	−logP
c1:c8	85	35	6.36	3.5	1.61	0.9	1.52	1.5	3.38	3.4
c1:c12	160	57	6.51	3.7	4.66	3.6	0.14	0.1	1.62	1.6
c2:c8	50	20	6.26	3.5	1.96	1.2	0.38	0.4	4.06	4.1
c3:c8	26	26	7.15	4.2	3.87	2.9	0.01	0.0	3.26	3.3
c3:c10	42	19	6.12	3.4	4.27	3.2	0.15	0.1	1.73	1.7
c4:c8	53	20	6.45	3.6	2.45	1.6	0.08	0.1	3.78	3.8
c5:c8	252	27	6.28	3.5	1.98	1.2	1.24	1.2	3.20	3.2
c6:c8	105	20	7.80	4.7	2.98	2.1	0.91	0.9	4.12	4.1
c8:c9	20	129	6.56	3.7	1.88	1.1	3.98	4.0	0.77	0.8
c8:c10	20	19	6.90	4.0	0.42	0.1	4.78	4.8	2.57	2.6
c8:c12	20	57	6.63	3.8	0.96	0.5	3.97	4.0	1.76	1.8
c8:c16	20	37	6.69	3.8	2.62	1.8	3.71	3.7	0.15	0.2
c8:c18	20	138	8.32	5.2	4.40	3.4	3.86	3.9	0.01	0

For each interaction presented, columns show the locus involved (c, chromosome), positions of the corresponding SNPs (pos1 and pos2), joint LOD score (LODjnt), LOD score of the interaction (LODint), and individual LOD scores for each individual QTL (LODq1 and LOD q2).

TABLE 2

Candidate genes for the TS locus on chromosome 8

Start	Stop	Symbol	Description	Human orthologs	GO
18595150	18803166	Mcph1	Microcephaly, primary autosomal recessive 1	MCPH1	Intracellular
18691314	18741528	Angpt2	Angiopoietin 2	ANGPT2	Angiogenesis
18846481	18884358	Agpat5	1-Acylglycerol-3-phosphate O-acyltransferase 5	AGPAT5	Metabolism
18932707	18950936	Xkr5	X Kell blood group precursor-related family, member 5	XKR5	Protein transport
23633994	23651364	Ckap2	Cytoskeleton associated protein 2	CKAP2	Cell cycle
23658405	23684142	Vps36	Vacuolar protein sorting 36 (yeast)	VPS36	Protein transport
23704045	23725434	Thsd1	Thrombospondin, type I, domain 1	THSD1	Inflammation
23841552	23864098	Slc25a15	Solute carrier family 25 (mitochondrial carrier ornithine transporter)	SLC25A15	Protein transport
23876965	23895022	Mrps31	Mitochondrial ribosomal protein S31	MRPS31	Transcription
23942327	24035157	Slc20a2	Solute carrier family 20, member 2	SLC20A2	Protein transport
24042646	24059303	Vdac3	Voltage-dependent anion channel 3	VDAC3	Anion transport
24089588	24093092	Dkk4	Dickkopf homolog 4 (Xenopus laevis)	DKK4	Wnt pathway
24093810	24118959	Polb	Polymerase (DNA directed), β	POLB	DNA repair
24125308	24172108	Ikbkb	Inhibitor of κB kinase β	IKBKB	Transcription
24223313	24248389	Plat	Plasminogen activator, tissue	PLAT	Proteolysis
24252900	24271176	Ap3m2	Adaptor-related protein complex 3, μ 2 subunit	AP3M2	Protein transport
24706892	24722557	Golga7	Golgi autoantigen, golgin subfamily a, 7	GOLGA7	Protein transport
24877063	24915177	Sfrp1	Secreted frizzled-related sequence protein 1	SFRP1	Wnt pathway
25135238	25528648	Zmat4	Zinc finger, matrin type 4	ZMAT4	Nucleic acid binding
26049686	26062554	Indo	Indoleamine-pyrrole 2,3 dioxygenase	INDO	Immunity
26067791	26140298	Adam18	A disintegrin and metallopeptidase domain 18	ADAM18	Cell differentiation
26142777	26191370	Adam3	a disintegrin and metallopeptidase domain 3 (cyritestin)	ADAM3	Cell adhesion
26198530	26289914	Adam5	A disintegrin and metallopeptidase domain 5	ADAM5	Cell adhesion
26301689	26414332	Adam32	A disintegrin and metallopeptidase domain 32	ADAM32	Proteolysis
26415170	26482339	Adam9	A disintegrin and metallopeptidase domain 9 (meltrin γ)	ADAM9	Proteolysis
26482825	26488804	Tm2d2	TM2 domain containing 2	TM2D2	Extracellular
26490473	26504507	Htra4	HtrA serine peptidase 4	HTRA4	NA
26506385	26567277	Plekha2	Pleckstrin homology domain-containing, family A (member 2	PLEKHA2	Metabolism
26620097	26666994	Tacc1	Transforming, acidic coiled-coil containing protein 1	TACC1	Cell cycle
26997826	27039466	Fgfr1	Fibroblast growth factor receptor 1	FGFR1	Angiogenesis
27067146	27185212	Whsc1l1	Wolf-Hirschhorn syndrome candidate 1-like 1 (human)	WHSC1L1	Transcription

Start and Stop indicate beginning and end of genes as base pairs on mouse chromosome 8. Symbol indicates symbol of the mouse gene. Description provides full name of the mouse gene. Human orthologs represent ortholog genes in human. GO, Gene ontology; NA, not available.